Symmetry-Controlled Ultrastrong Phonon–Photon Coupling in a Terahertz Cavity

Dasom Kim,¹ Maxime Dherbécourt,² Sae R. Endo,^{3,4} Geon Lee,⁵ Ayush Agrawal,⁶ Sunghwan Kim,⁷ Wen-Hua Wu,^{1,8} Aditya D. Mohite,^{3,6,9} Minah Seo,^{5,10} David Hagenmüller,² and Junichiro Kono*^{1,3,9,11,12} Department of Electrical and Computer Engineering, Rice University, Houston, TX 77005, USA

(*Electronic mail: kono@rice.edu)

(Dated: 21 November 2025)

Optical cavities provide a powerful means to engineer light–matter hybrid states by coupling confined electromagnetic fields with matter excitations. Achieving *in situ* control of the coupling strength is essential for investigating how such hybridization evolves with the coupling strength. In this work, we use a symmetry-changing structural phase transition in lead halide perovskites to reversibly tune the phonon–photon coupling strength, leveraging the fact that their phonon frequencies and oscillator strengths are dictated by lattice symmetry. Terahertz time-domain spectroscopy of MAPbI₃ embedded in nanoslot cavities reveals three polariton branches above the critical temperature $T_{\rm c} \simeq 162.5 \, {\rm K}$, and the emergence of an additional branch below $T_{\rm c}$, activated by a new phonon mode in the low-temperature phase. The full dispersion is accurately reproduced using a multimode Hopfield model, confirming that all normalized coupling strengths remain in the ultrastrong coupling regime. These results demonstrate symmetry-controlled tuning of ultrastrong coupling via phonon engineering in optical cavities.

I. INTRODUCTION

Light confined in optical cavities can strongly interact with collective excitations in solids, forming mixed light—matter hybrids known as polaritons. The ultrastrong coupling (USC) regime is reached when the light—matter coupling strength *g* becomes a sizable fraction of the bare excitation frequency^{1,2}. USC has now been demonstrated in a variety of solid-state platforms, including Landau polaritons^{3–6}, magnetic systems^{7–9}, and phonon polaritons^{10–14}. In this nonperturbative regime, the ground state is predicted to be strongly dressed by vacuum fluctuations, giving rise to associated phenomena such as squeezed ground states^{15,16} and to modifications of vibrational^{17,18}, electronic^{19,20}, and magnetic properties^{9,21,22}.

A central challenge in rigorously identifying such polaritonic effects is to achieve the ability to vary the coupling strength *g in situ*, so that changes in material properties can be directly linked to changes in *g*. In most cavity–matter systems, however, *g* is fixed once the cavity geometry and

mode volume are defined, limiting experimental control. Attempts to tune g by continuously modifying intrinsic material parameters—such as carrier density²³ or spin density²²—introduce ambiguity, since conventional material responses cannot be cleanly separated from genuine polaritonic effects.

An alternative strategy is to exploit a well-defined phase transition as a built-in tuning parameter 18 . Lead halide perovskites (MAPbX3; MA = CH3NH3+, X = Cl, Br, I), widely investigated for photovoltaic applications 24 , are particularly well suited in this regard. In MAPbI3, temperature-driven structural transitions between orthorhombic, tetragonal, and cubic phases $^{25-27}$ lead to discrete changes in lattice symmetry and phonon spectra, providing a clear reference against which the influence of light–matter hybridizations on phase stability, dynamics, or material properties can be assessed.

Lead halide perovskites have recently emerged as promising systems for realizing USC between photons and optical phonons in terahertz (THz) metamaterial cavities 10,12,14. While previous studies have demonstrated USC within a single structural phase, and one recent work has investigated

²⁾Institut de Physique et Chimie des Matériaux de Strasbourg (UMR 7504), Université de Strasbourg and CNRS, Strasbourg, 67200, France

³⁾Smalley-Curl Institute, Rice University, Houston, TX 77005, USA

⁴⁾Department of Applied Physics and Physico-Informatics, Keio University, Yokohama 223-8522, Japan

⁵⁾Sensor System Research Center, Korea Institute of Science and Technology, Seoul, 02792, Republic of Korea

⁶⁾Department of Chemical and Biomolecular Engineering, Rice University, Houston, TX 77005, USA

⁷⁾Department of Physics, Ulsan National Institute of Science and Technology (UNIST), Ulsan, 44919, Republic of Korea

⁸⁾ Applied Physics Graduate Program, Smalley–Curl Institute, Rice University, Houston, TX 77005,

⁹⁾Department of Materials Science and NanoEngineering, Rice University, Houston, TX 77005, USA

¹⁰⁾Department of Physics, Sogang University, Seoul, 04107, Republic of Korea

¹¹⁾Rice Advanced Materials Institute, Rice University, Houston, TX 77005, USA

¹²⁾Department of Physics and Astronomy, Rice University, Houston, TX 77005, USA

phonon–photon coupling across a phase transition in the strong-coupling regime²⁸, the evolution of polariton formation under USC across a symmetry-changing transition remains largely unexplored.

In this work, we use a structural phase transition in MAPbI₃ thin films as a reversible control knob to modulate g in subwavelength-mode-volume THz nanoslot cavities. Temperature-dependent THz time-domain spectroscopy (THz-TDS) reveals the emergence of an additional polariton branch below the critical temperature $T_c \simeq 162.5 \,\mathrm{K}$, consistent with the activation of a new phonon mode in the orthorhombic phase. The full polariton dispersion across the transition is accurately reproduced using a multimode Hopfield model, confirming that all normalized coupling strengths remain in the USC regime. Within our experimental precision, the transition temperature is unchanged, indicating that light-matter hybridization does not measurably affect phase stability under the present coupling conditions. These results provide new insight into multimode polariton formation across phase boundaries and establish a pathway for engineering functional material properties in perovskites and related systems via ultrastrong light-matter interactions.

II. RESULTS

At room temperature, MAPbI₃ adopts a tetragonal structure and exhibits two phonon modes in the THz range, originating from the rocking and stretching vibrations of the Pb–I bonds^{25–27}. Upon cooling, the material undergoes a structural phase transition at $T_{\rm c}\approx 162.5\,\rm K$ from tetragonal to orthorhombic symmetry. This symmetry change modifies the vibrational spectrum of the Pb–I framework, causing the two tetragonal-phase phonon modes to split into four distinct modes in the orthorhombic phase²⁷.

To verify this behavior, we performed THz-TDS on a 200 nm-thick bare MAPbI $_3$ film. Figure 1 (upper panel) shows the THz transmission spectra in the two structural phases. In the tetragonal phase (165 K), two absorption dips are observed at approximately 0.95 THz and 1.78 THz, corresponding to the TO $_1$ and TO $_2$ phonon modes. Below T_c , the lower mode splits into two peaks at 0.77 THz and 0.98 THz, while the TO $_2$ mode appears unchanged. The expected splitting of the TO $_2$ mode is not resolved in the spectra because the oscillator strength of the fourth mode is significantly weaker than that of the original TO $_2$ mode in this temperature range²⁷.

Because the MAPbI₃ film thickness is much smaller than the THz wavelength, the bare THz electromagnetic field couples only weakly to the phonons. To reach the USC regime, we employ nanoslot cavities that strongly enhance the electric field inside the slots^{29,30}. The cavities were fabricated as arrays of nanoslots with a width of $w = 500\,\mathrm{nm}$ on quartz substrates using standard photolithography and lift-off techniques; see Fig. 2 for fabrication details. Figure 1 (lower panel) shows a representative transmittance spectrum for a nanoslot with length $l = 60\,\mathrm{\mu m}$, featuring a single peak at the resonance frequency.

Next, we deposited 200-nm-thick MAPbI₃ films onto the

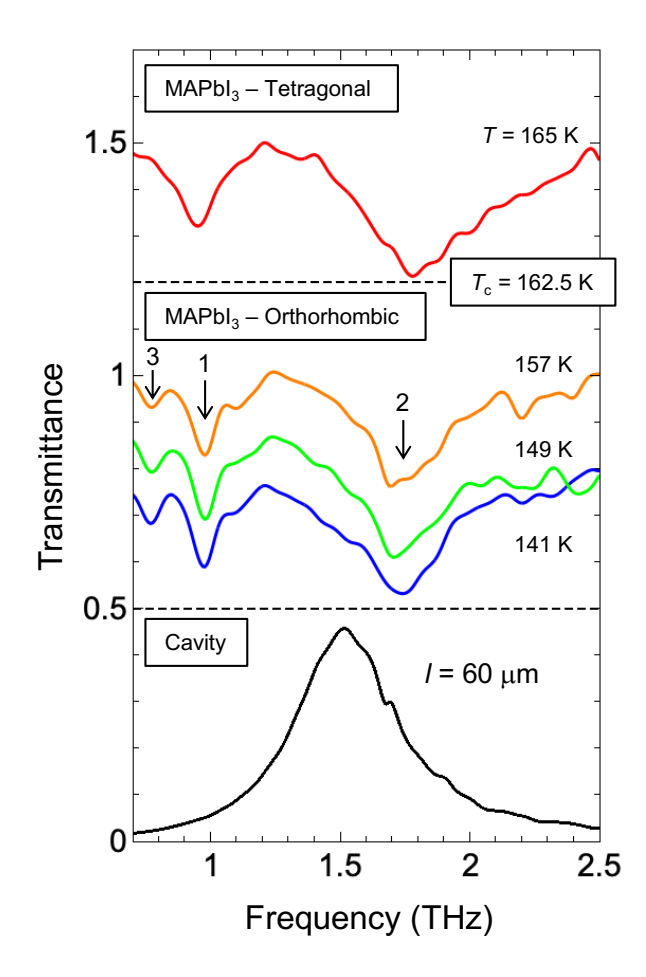


FIG. 1. Temperature-dependent terahertz transmission spectra of MAPbI₃. Upper: Bare MAPbI₃ film showing two phonon modes at around 0.95 THz and 1.78 THz in the tetragonal phase (165 K) and three modes in the orthorhombic phase (below $T_c = 162.5$ K) due to structural splitting of Pb–I vibrations. Lower: Transmission of a nanoslot cavity ($l = 60 \, \mu m$) exhibiting a resonance at 1.52 THz.

nanoslot arrays. A schematic of the resulting MAPbI₃–nanoslot hybrid structures is shown in Fig. 2(a). To tune the cavity resonance, we fabricated samples with different cavity lengths ($l=30,40,50,60,70,80,120,160\,\mu m$). The dependence of the cavity frequency on l is plotted in Fig. 2(b). Because the resonance is primarily determined by the nanoslot geometry, the cavity frequency decreases as l increases. By varying l, we therefore control the detuning between the bare cavity mode and the phonon mode, and consequently the degree of light–matter hybridization for each phonon branch.

We carried out THz-TDS measurements on the hybrid systems at various temperatures across T_c . Time-domain signals from the samples and a quartz reference were recorded and Fourier transformed to obtain transmission spectra in the range 0.2–3 THz. Figure 2(c) presents color maps of the normalized transmittance for hybrid systems with different cavity frequencies ω_c (set by l) in the tetragonal phase (left, 165 K) and orthorhombic phase (right, 151 K). In the tetragonal phase (165 K), three polariton branches are observed, consistent with previous results¹⁴. These features correspond to the

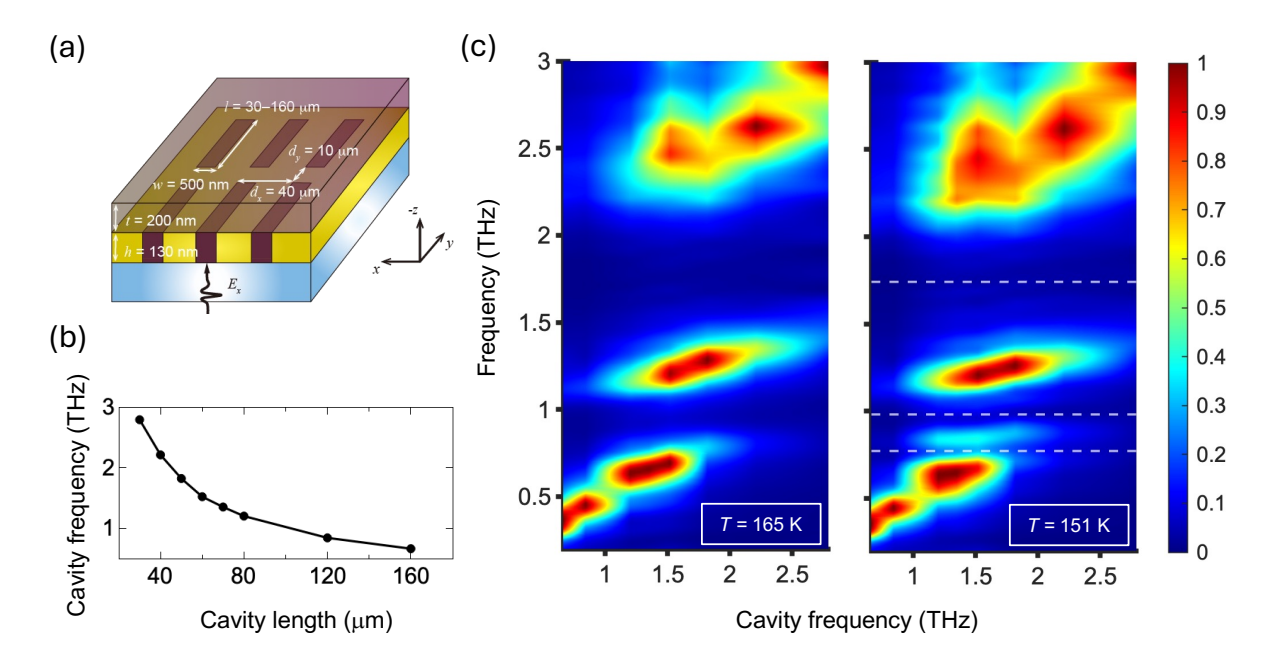


FIG. 2. THz transmission maps of MAPbI₃-nanoslot hybrid systems. (a) Schematic illustration of the hybrid structure. (b) The dependence of the cavity resonance frequency on nanoslot length l. (c) Normalized transmittance color maps at 165 K (tetragonal) and 151 K (orthorhombic), respectively. Three polaritonic branches, lower (LP), middle (MP), and upper (UP), arise from the ultrastrong coupling of the cavity mode with phonon modes TO_1 and TO_2 ; below T_c a new branch appears near 0.83 THz, indicating coupling with the emergent third phonon mode.

lower- (LP), middle- (MP), and upper-polariton (UP) modes arising from the hybridization of the TO₁ and TO₂ phonons with the cavity mode, as shown below. The larger oscillator strength of TO₂ leads to a correspondingly larger Rabi splitting. In the orthorhombic phase (151 K), an additional branch appears near 0.83 THz for 1.2 THz $\leq \omega_c \leq$ 1.8 THz. The three branches below 1.5 THz are now separated by the two lowerfrequency phonon modes (labeled 1 and 3 in Fig. 1), as indicated by the lower dashed white lines. We show below that the additional polariton branch arises from the coupling between the cavity mode and the third phonon mode, which becomes active in the orthorhombic phase, at low cavity frequencies, and with the first phonon mode at high cavity frequencies. In addition, the UP branch becomes broader and red-shifted, a behavior attributed to the emergence of the fourth phonon mode.

The formation of phonon-polaritons can be described theoretically by a multimode Hopfield model³¹. Following the approach of Ref. [14], we start from the microscopic Hamiltonian

$$H = \hbar \omega_{c} a^{\dagger} a + \sum_{\lambda} \hbar \omega_{\lambda} b_{\lambda}^{\dagger} b_{\lambda} - i \sum_{\lambda} \hbar g_{\lambda} (b_{\lambda} - b_{\lambda}^{\dagger}) (a + a^{\dagger})$$
$$+ \sum_{\lambda} \frac{\hbar g_{\lambda}^{2}}{\omega_{\lambda}} (a + a^{\dagger})^{2}, \tag{1}$$

where a (a^{\dagger}) is the annihilation (creation) operator of the cavity photon mode with frequency ω_c , and b_{λ} (b_{λ}^{\dagger}) the annihilation (creation) operator of the phonon mode labeled by λ and with frequency ω_{λ} . For temperatures above T_c we include two phonon modes, $\lambda=1,2$, corresponding to the TO₁ and TO₂

transverse optical phonons of the perovskite, while below $T_{\rm c}$ an additional mode $\lambda=3$ is incorporated to account for the phonon that appears in the orthorhombic phase. The first two terms in Eq. (1) describe the free energy of the cavity field and of the phonon modes, respectively. The third term represents the light–matter interaction, with coupling strength λ given by $g_{\lambda}=v_{\lambda}\sqrt{\omega_{\lambda}/\omega_{\rm c}}/2$. Here, v_{λ} corresponds to the effective ionic plasma frequency of mode λ , characterizing the effective charges associated with the Pb²⁺ and I⁻ ions participating in the lattice vibration. The final term is the diamagnetic (or A^2) contribution, which becomes important in the USC regime (see Ref. [14] for derivation details).

Equation (1) can be diagonalized by performing a Hopfield-Bogoliubov transformation and introducing bosonic polaritonic annihilation operators of the form $p_{\alpha} = w_{\alpha} a +$ $\sum_{\lambda} x_{\lambda,\alpha} b_{\lambda} + y_{\alpha} a^{\dagger} + \sum_{\lambda} z_{\lambda,\alpha} b_{\lambda}^{\dagger}$, where w_{α} , $x_{\lambda,\alpha}$, y_{α} , and $z_{\lambda,\alpha}$ are complex coefficients. These operators allow the Hamiltonian to be expressed as $H = \sum_{\alpha} \hbar \Omega_{\alpha} p_{\alpha}^{\dagger} p_{\alpha}$, with Ω_{α} denoting the polaritonic eigenfrequencies. The index α runs over the total number of polaritonic modes, i.e., the single cavity degree of freedom together with the phonon modes present in the phase under consideration. In the USC regime the diamagnetic (A^2) contribution in Eq. (1) becomes significant and can no longer be neglected, as well as the anti-resonant components of the Hopfield transformation, contained in the coefficients y_{α} and $z_{\lambda,\alpha}$. Accordingly, each polaritonic mode α contains contributions from each individual phonon TO_{λ} quantified by the phonon fraction $\mathscr{F}_{\lambda,\alpha}^{\rm ph} = |x_{\lambda,\alpha}|^2 - |z_{\lambda,\alpha}|^2$, and from the cavity photons through the fraction $\mathscr{F}_{\alpha}^{\text{pt}} = |w_{\alpha}|^2 - |y_{\alpha}|^2$. Here, both phononic and photonic weights ex-

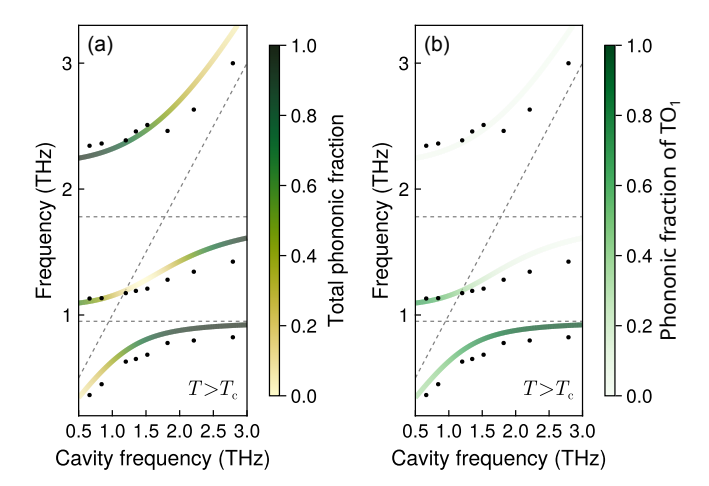


FIG. 3. Polaritonic dispersion as a function of the cavity frequency for $T=165\,\mathrm{K}>T_\mathrm{c}$, calculated by numerical diagonalization of Eq. (1), and compared with the experimental data (black markers). (a) The colour scale encodes the photonic (yellow) and phononic (green) content of each polaritonic eigenmode α , quantified by the fractions $\sum_{\lambda} \mathscr{F}^{\mathrm{ph}}_{\lambda,\alpha}$ and $\mathscr{F}^{\mathrm{pt}}_{\alpha}$, respectively. In (b), the colours scale represents the phononic contribution from the TO₁ mode to each polariton branch $\mathscr{F}^{\mathrm{ph}}_{\lambda=1,\alpha}$. (a, b) Dashed lines indicate the uncoupled cavity and bare phonon-mode frequencies. The transverse-optical phonons are located at $\omega_1=0.95\,\mathrm{THz}$ and $\omega_2=1.78\,\mathrm{THz}$. The coupling strengths g_{λ} reported in the main text are then obtained by fitting the calculated dispersion to these experimental data.

plicitly account for the contributions of both the resonant and anti-resonant Hopfield coefficients.

Numerical diagonalization of the Hamiltonian was performed for a range of cavity frequencies ω_c , and the resulting polaritonic dispersions were fitted to the experimental data by varying the light–matter coupling strengths g_{λ} , while using the experimentally determined phonon frequencies ω_{λ} as fixed inputs (see Figs. 3 and 4). Each coupling strength g_{λ} is measured numerically at resonance between the cavity and the corresponding TO frequency, that is $\omega_c = \omega_{\lambda}$, for every phonon mode λ . From this procedure, we obtain the following normalized couplings. Above the transition temperature T_c (tetragonal phase) the TO_1 and TO_2 modes yield $g_1/\omega_1 = 0.36$ and $g_2/\omega_2 = 0.35$. Below T_c (orthorhombic phase), where an additional transverse-optical mode TO₃ is present, the extracted values are $g_1/\omega_1 = 0.28$, $g_2/\omega_2 = 0.36$, and $g_3/\omega_3 = 0.25$. All reported couplings lie within the USC regime with the nanoslot resonator, which underlines the necessity of retaining the diamagnetic (A^2) term in Eq. (1) as well as the anti-resonant terms. The temperature dependence of the extracted couplings (Figs. 3 and 4) reveals a marked variation at the structural phase transition. While the coupling of the TO₂ mode is essentially temperature independent, the coupling of the TO₁ mode decreases by approximately 30% upon cooling from the tetragonal to the orthorhombic phase. The emergent TO_3 mode below T_c exhibits a coupling strength comparable to that of TO₁. These changes are attributed to the lattice reorganization across the phase transition, which modifies the effective ionic plasma frequencies v_{λ} entering

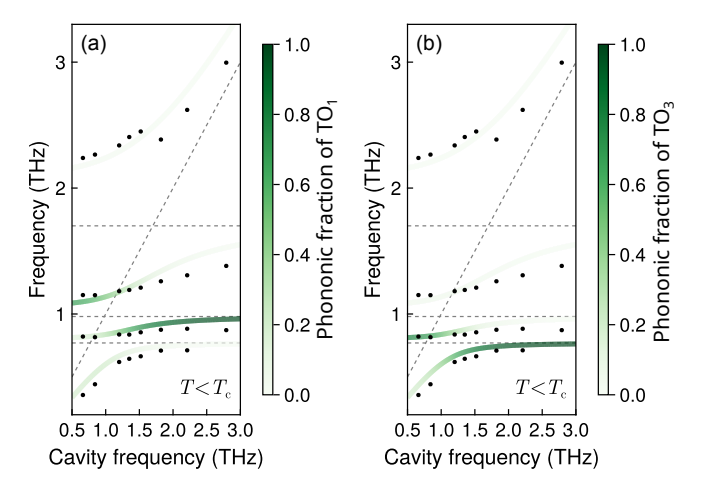


FIG. 4. Polaritonic dispersion as a function of the cavity frequency, calculated by numerical diagonalization of Eq. (1), and compared with the experimental data (black markers), simirally as Fig. 3, but for $T=151\,\mathrm{K} < T_\mathrm{c}$. The colours scale represents the phononic contribution from the TO₁ (a) and TO₃ (b) modes to each polariton branch. Here, the transverse–optical phonons are located at $\omega_1=0.98\,\mathrm{THz}$, $\omega_2=1.7\,\mathrm{THz}$ and $\omega_3=0.77\,\mathrm{THz}$.

the light–matter interaction, while preserving the system in the USC regime. Now examining the phononic and photonic weights, as shown in Fig. 3 above the critical temperature, we find that the TO_1 mode predominantly contributes to the phononic character of the two lowest polaritonic branches. Below T_c (Fig. 4), the emergence of the new TO_3 mode leads to a redistribution of the total phononic weight between the LP and the newly formed MP branch just below 1 THz. While this branch is primarily composed of the TO_1 mode at high cavity frequencies, it mainly consists of the TO_3 mode at low cavity frequencies.

To examine whether the formation of light-matter hybrids in the USC regime influences the structural phase transition in MAPbI3, we analyzed the evolution of polariton frequencies as a function of temperature for two different cavity frequencies $\omega_c = 1.2\,\text{THz}$ and 2.2 THz. We note that the bare film response is too weak to resolve such detailed temperature evolution under our experimental conditions, making the cavity-coupled system essential for sensitively tracking the transition through polaritonic features. In Fig. 3(a) $(T > T_c)$, the photonic weight of each polariton branch, indicated by the color scale, reveals that for $\omega_c = 1.2 \, \text{THz}$, the two lower polaritonic branches possess the highest photonic fraction, whereas at $\omega_c = 2.2 \, \text{THz}$, the upper polariton (UP) branch carries most of the photonic weight. Below the critical temperature $[T < T_c$, see Fig. 4], these relative trends are preserved. However, the emergence of two new polariton modes below 1 THz leads to a partial transfer of phononic weight from the original LP branch, thereby reducing their individual phonon contributions. As shown in Fig. 5, the phase transition from the orthorhombic to tetragonal phase is clearly tracked by the spectral evolution and the disappearance of polariton branches across $T_c \simeq 162.5$ K, indicated by the vertical dashed lines. In both cases, the UP branches show the sat-

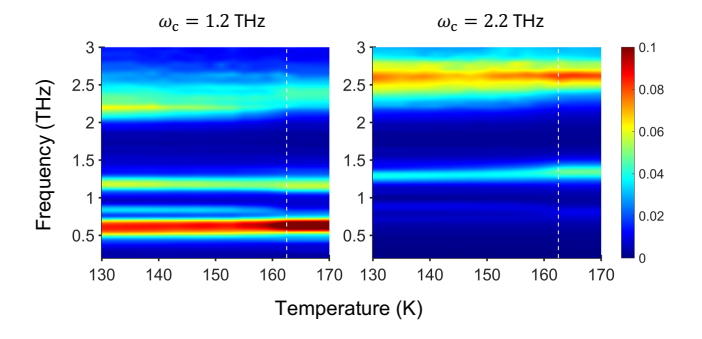


FIG. 5. Temperature-dependent THz transmission spectra of hybrid systems with cavity frequencies $\omega_{\rm c}=1.2$ THz and 2.2 THz. Each color map shows the evolution of polariton branches as the sample is heated through the tetragonal–orthorhombic transition near $T_{\rm c}\simeq 162.5$ K, indicated by vertical dashed lines. Some of the polariton branches gradually disappear or saturate above $T_{\rm c}$. Despite the markedly different light–matter hybridization conditions, the transition occurs at approximately the same temperature within the 2 K experimental uncertainty.

uration behavior at above 162.5 K. Similarly, other polariton branches show the disappearance or saturation across T_c . Despite the markedly different hybridization, the disappearance of the orthorhombic-phase polariton features occurred at approximately the same T_c within our experimental resolution of 2 K. These results suggest that, within our experimental limit, the formation of phonon-polaritons in the USC regime does not noticeably alter the structural phase transition temperature in MAPbI₃. Nonetheless, the possibility of more subtle cavity-induced effects, such as modified lattice fluctuations, cannot be excluded and may warrant further investigation under different coupling geometries or stronger vacuum-field confinement. In particular, coupling to a soft phonon mode that approaches zero frequency at the phase boundary could provide an intriguing route to explore cavity-modified critical behavior.

III. CONCLUSION

In summary, we have demonstrated symmetry-controlled multimode USC between THz cavity photons and optical phonons in hybrid MAPbI₃–nanoslot systems. Above T_c , the tetragonal phase exhibits two infrared-active phonons that hybridize with the cavity mode to form three distinct polariton branches. Below T_c , the transition to the orthorhombic phase introduces an additional phonon mode, leading to the emergence of a new polariton branch and a redistribution of the coupling strength. Overall, this work establishes halide perovskites as a versatile platform for exploring light–matter interactions with the *in-situ* control of the coupling strength g, paving the way toward phonon-engineered quantum optoelectronic materials.

ACKNOWLEDGMENTS

D.K. and J.K. acknowledge support from the U.S. Army Research Office (through Award No. W911NF2110157), the W. M. Keck Foundation (through Award No. 995764), the Gordon and Betty Moore Foundation (through Grant No. 11520), and the Robert A. Welch Foundation (through Grant No. C-1509). M.D. and D.H. acknowledge support from the Interdisciplinary Thematic Institute QMat, as part of the ITI 2021-2028 program of the University of Strasbourg, CNRS, and Inserm, supported by IdEx Unistra (Project No. ANR 10 IDEX 0002), and by SFRI STRAT'US Projects No. ANR-20-SFRI-0012 and No. ANR-17-EURE-0024 under the framework of the French Investments for the Future Program.

AUTHOR CONTRIBUTIONS

J.K. supervised the project. D.K. conceived the project, built the THz spectroscopy setup, performed THz measurements, and analyzed the experimental data under the guidance of J.K. S.R.E. and W.-H.W. helped THz measurements. G.L., S.K., and D.K. designed and fabricated the nanoslot cavities under the guidance of M.S. M.D. and D.H. developed the theoretical model and performed the calculations. A.A. grew the perovskite films under the guidance of A.D.M. D.K., M.D., S.R.E., D.H., and J.K. wrote the manuscript. All authors discussed the results and commented on the manuscript.

DATA AVAILABILITY STATEMENT

Data available on request from the authors.

¹A. Frisk Kockum, A. Miranowicz, S. De Liberato, S. Savasta, and F. Nori, "Ultrastrong coupling between light and matter," Nat. Rev. Phys. **1**, 19–40 (2019)

²P. Forn-Díaz, L. Lamata, E. Rico, J. Kono, and E. Solano, "Ultrastrong coupling regimes of light–matter interaction," Rev. Mod. Phys. **91**, 025005 (2019).

³G. Scalari, C. Maissen, D. Turčinková, D. Hagenmüller, S. De Liberato, C. Ciuti, C. Reichl, D. Schuh, W. Wegscheider, M. Beck, and J. Faist, "Ultrastrong coupling of the cyclotron transition of a 2D electron gas to a thz metamaterial," Science 335, 1323–1326 (2012).

⁴Q. Zhang, M. Lou, X. Li, J. L. Reno, W. Pan, J. D. Watson, M. J. Manfra, and J. Kono, "Collective non-perturbative coupling of 2D electrons with high-quality-factor terahertz cavity photons," Nat. Phys. **12**, 1005–1011 (2016).

⁵X. Li, M. Bamba, Q. Zhang, S. Fallahi, G. C. Gardner, W. Gao, M. Lou, K. Yoshioka, M. J. Manfra, and J. Kono, "Vacuum Bloch–Siegert shift in Landau polaritons with ultra-high cooperativity," Nat. Photon. 12, 324–329 (2018).

⁶F. Tay, A. Mojibpour, S. Sanders, S. Liang, H. Xu, G. C. Gardner, A. Baydin, M. J. Manfra, A. Alabastri, D. Hagenmüller, and J. Kono, "Multimode ultrastrong coupling in three-dimensional photonic-crystal cavities," Nat. Commun. 16, 3603 (2025).

⁷X. Li, M. Bamba, N. Yuan, Q. Zhang, Y. Zhao, M. Xiang, K. Xu, Z. Jin, W. Ren, G. Ma, S. Cao, D. Turchinovich, and J. Kono, "Observation of Dicke cooperativity in magnetic interactions," Science 361, 794–797 (2018).

⁸T. Makihara, K. Hayashida, G. T. Noe II, X. Li, N. Marquez Peraca, X. Ma, Z. Jin, W. Ren, G. Ma, I. Katayama, J. Takeda, H. Nojiri, D. Turchinovich,

- S. Cao, M. Bamba, and J. Kono, "Ultrastrong magnon-magnon coupling dominated by antiresonant interactions," Nat. Commun. 12, 3115 (2021).
- ⁹D. Kim, S. Dasgupta, X. Ma, J.-M. Park, H.-T. Wei, X. Li, L. Luo, J. Doumani, W. Yang, D. Cheng, R. H. J. Kim, H. O. Everitt, S. Kimura, H. Nojiri, J. Wang, S. Cao, M. Bamba, K. R. A. Hazzard, and J. Kono, "Observation of the magnonic Dicke superradiant phase transition," Sci. Adv. 11, eadt1691 (2025).
- ¹⁰H. S. Kim, N. Y. Ha, J.-Y. Park, S. Lee, D.-S. Kim, and Y. H. Ahn, "Phonon-polaritons in lead halide perovskite film hybridized with THz metamaterials," Nano Lett. 20, 6690–6696 (2020).
- ¹¹M. Barra-Burillo, U. Muniain, S. Catalano, M. Autore, F. Casanova, L. E. Hueso, J. Aizpurua, R. Esteban, and R. Hillenbrand, "Microcavity phonon polaritons from the weak to the ultrastrong phonon–photon coupling regime," Nature Communications 12, 6206 (2021).
- ¹²Y. Roh, M. Chae, J. Oh, W. Kim, M.-Y. Ryu, M. Seo, and J. Jeong, "Ultrastrong coupling enhancement with squeezed mode volume in terahertz nanoslots," Nano Lett. 23, 7086–7091 (2023).
- ¹³ A. Baydin, M. Manjappa, S. S. Mishra, H. Xu, J. Doumani, F. Tay, D. Kim, P. H. O. Rappl, E. Abramof, R. Singh, F. G. G. Hernandez, and J. Kono, "Terahertz cavity phonon polaritons in lead telluride in the deep-strong coupling regime," arXiv:2501.10856 (2025), 2501.10856 [physics.optics].
- ¹⁴D. Kim, J. Hou, G. Lee, A. Agrawal, S. Kim, H. Zhang, D. Bao, A. Baydin, W. Wu, F. Tay, S. Huang, E. E. M. Chia, D.-S. Kim, M. Seo, A. D. Mohite, D. Hagenmüller, and J. Kono, "Multimode phonon-polaritons in lead-halide perovskites in the ultrastrong coupling regime," Nature Communications 16, 8658 (2025).
- ¹⁵C. Ciuti, G. Bastard, and I. Carusotto, "Quantum vacuum properties of the intersubband cavity polariton field," Phys. Rev. B 72, 115303 (2005).
- ¹⁶ K. Hayashida, T. Makihara, N. M. Peraca, D. F. Padilla, H. Pu, J. Kono, and M. Bamba, "Perfect intrinsic squeezing at the superradiant phase transition critical point," Sci. Rep. 13, 2526 (2023).
- ¹⁷S. Wang, A. Mika, J. A. Hutchison, C. Genet, A. Jouaiti, M. W. Hosseini, and T. W. Ebbesen, "Phase transition of a perovskite strongly coupled to the vacuum field," Nanoscale 6, 7243–7248 (2014).
- ¹⁸G. Jarc, S. Y. Mathengattil, A. Montanaro, F. Giusti, E. M. Rigoni, R. Sergo, F. Fassioli, S. Winnerl, S. Dal Zilio, D. Mihailovic, P. Prelovšek, M. Eckstein, and D. Fausti, "Cavity-mediated thermal control of metal-to-insulator transition in 1T-TaS₂," Nature 622, 487–492 (2023).
- ¹⁹F. Appugliese, J. Enkner, G. L. Paravicini-Bagliani, M. Beck, C. Reichl, W. Wegscheider, G. Scalari, C. Ciuti, and J. Faist, "Breakdown of topological protection by cavity vacuum fields in the integer quantum Hall effect," Science 375, 1030–1034 (2022).
- ²⁰A. Thomas, E. Devaux, K. Nagarajan, T. Chervy, M. Seidel, G. Rogez, J. Robert, M. Drillon, T. T. Ruan, S. Schlittenhardt, M. Ruben, D. Ha-

- genmüller, S. Schütz, J. Schachenmayer, C. Genet, G. Pupillo, and T. W. Ebbesen, "Exploring superconductivity under strong coupling with the vacuum electromagnetic field," The Journal of Chemical Physics **162**, 134701 (2025).
- ²¹A. Thomas, E. Devaux, K. Nagarajan, G. Rogez, M. Seidel, F. Richard, C. Genet, M. Drillon, and T. W. Ebbesen, "Large enhancement of ferromagnetism under a collective strong coupling of YBa₂Cu₃O_{7-x} nanoparticles," Nano Letters 21, 4365–4370 (2021).
- ²²T. E. Kritzell, J. Doumani, T. Asano, S. Yamada, F. Tay, H. Xu, H. Yan, I. Katayama, J. Takeda, A. Nevidomskyy, H. Nojiri, M. Bamba, A. Baydin, and J. Kono, "Zeeman polaritons as a platform for probing Dicke physics in condensed matter," arXiv [quant-ph] (2024), arXiv:2409.17339 [quant-ph].
- ²³G. L. Paravicini-Bagliani, G. Scalari, F. Valmorra, J. Keller, C. Maissen, M. Beck, and J. Faist, "Gate and magnetic field tunable ultrastrong coupling between a magnetoplasmon and the optical mode of an LC cavity," Phys. Rev. B 95, 205304 (2017).
- ²⁴ A. Kojima, K. Teshima, Y. Shirai, and T. Miyasaka, "Organometal halide perovskites as visible-light sensitizers for photovoltaic cells," J. Am. Chem. 131, 6050–6051 (2009).
- ²⁵A. Poglitsch and D. Weber, "Dynamic disorder in methylammoniumtrihalogenoplumbates (II) observed by millimeter-wave spectroscopy," The Journal of Chemical Physics 87, 6373–6378 (1987).
- ²⁶N. Onoda-Yamamuro, T. Matsuo, and H. Suga, "Calorimetric and IR spectroscopic studies of phase transitions in methylammonium trihalogeno-plumbates (II)†," Journal of Physics and Chemistry of Solids 51, 1383–1395 (1990).
- ²⁷C. La-o-vorakiat, H. Xia, J. Kadro, T. Salim, D. Zhao, T. Ahmed, Y. M. Lam, J.-X. Zhu, R. A. Marcus, M.-E. Michel-Beyerle, and E. E. M. Chia, "Phonon mode transformation across the orthohombic-tetragonal phase transition in a lead iodide perovskite CH₃NH₃PbI₃: A terahertz time-domain spectroscopy approach," J. Phys. Chem. Lett. 7, 1–6 (2016).
- ²⁸G. Jarc, S. Y. Mathengattil, A. Montanaro, E. M. Rigoni, S. Dal Zilio, and D. Fausti, "Multimode vibrational coupling across the insulator-to-metal transition in 1T-TaS₂ in thz cavities," The Journal of Chemical Physics 161, 154711 (2024).
- ²⁹M. A. Seo, H. R. Park, S. M. Koo, D. J. Park, J. H. Kang, O. K. Suwal, S. S. Choi, P. C. M. Planken, G. S. Park, N. K. Park, Q. H. Park, and D.-S. Kim, "Terahertz field enhancement by a metallic nano slit operating beyond the skin-depth limit," Nat. Photon. 3, 152–156 (2009).
- ³⁰D. Kim, J. Jeong, G. Choi, Y.-M. Bahk, T. Kang, D. Lee, B. Thusa, and D.-S. Kim, "Giant field enhancements in ultrathin nanoslots above 1 terahertz," ACS Photonics 5, 1885–1890 (2018).
- ³¹J. J. Hopfield, "Theory of the contribution of excitons to the complex dielectric constant of crystals," Physical Review 112, 1555–1567 (1958).